



OPEN

Nano-scaffold containing functional motif of stromal cell-derived factor 1 enhances neural stem cell behavior and synaptogenesis in traumatic brain injury

Mohammad Amin Bayat Tork^{1,2,9}, Mohsen Saberifar^{1,2,9}, Hamed Joneidi Yekta^{3,9}, Mehrdad Hajinejad⁴, Hassan Hosseini Ravandi⁵, Ali Gorji^{5,6,7}✉ & Sajad Sahab Negah^{1,2,5,8}✉

Traumatic brain injury (TBI) is a leading cause of mortality and morbidity worldwide, presenting a significant challenge due to the lack of effective therapies. Neural stem cells (NSCs) have shown promising potential in preclinical studies as a therapy for TBI. However, their application is limited by challenges related to poor survival and integration within the injured brain. This study investigated the effect of a novel nano-scaffold containing stromal cell-derived factor 1 (SDF-1) on NSC behavior and synaptogenesis after TBI. Using an innovative design, we successfully fabricated a nano-scaffold with Young's modulus of approximately 3.21 kPa, which aligns closely with the mechanical properties exhibited by neural tissue. This achievement marks the first time such a scaffold has been created and has promising implications for its potential use in neural tissue engineering applications. Our findings demonstrate that the nano-scaffold enhances NSC proliferation, migration, and differentiation capacity *in vitro*. Moreover, when transplanted into the injured brain, the nano-scaffold promotes the survival and integration of NSCs, leading to increased synaptogenesis and functional recovery. These findings suggest that using the novel nano-scaffold containing SDF-1 could provide a promising approach to treating TBI by improving NSC behavior and promoting synaptogenesis.

Keywords Brain injury, Tissue engineering, Nano-scaffold, CXCL12, Synaptic transmission

Traumatic brain injury (TBI) is a devastating condition that affects millions of people worldwide each year^{1,2}. TBI often results in significant neuronal damage, including the loss of synaptic connections, which can lead to long-term functional deficits³. One of the main challenges in treating TBI is the limited capacity of the brain to regenerate damaged tissue^{4,5}. In recent years, however, there has been growing interest in using neural tissue engineering as a promising strategy to promote neural tissue repair and regeneration^{6,7}. This approach involves the development of biomaterials, scaffolds, and other devices designed to support the growth and differentiation of neural stem cells (NSCs), ultimately leading to the development of new neural tissue^{8,9}.

Hydrogels have emerged as a particularly promising tool in neural tissue engineering for TBI^{10–14}. These materials mimic the structure and function of the extracellular matrix (ECM), which is a complex network of proteins and other molecules that support cell growth and differentiation^{15,16}. By creating hydrogels that

¹Neuroscience Research Center, Mashhad University of Medical Sciences, Mashhad, Iran. ²Department of Neuroscience, Faculty of Medicine, Mashhad University of Medical Sciences, Mashhad, Iran. ³New Technologies Research Center, Amirkabir University of Technology, Tehran, Iran. ⁴Qaen Faculty of Medical Science, Birjand University of Medical Sciences, Birjand, Iran. ⁵Shefa Neuroscience Research Center, Khatam Alanbia Hospital, Tehran, Iran. ⁶Department of Neurosurgery, Westfälische Wilhelms-Universität, 48149 Münster, Germany. ⁷Epilepsy Research Center, Westfälische Wilhelms-Universität Münster, 48149 Münster, Germany. ⁸Multiple Sclerosis Research Center, Neuroscience Institute, Tehran University of Medical Sciences, Tehran, Iran. ⁹Mohammad Amin Bayat Tork, Mohsen Saberifar and Hamed Joneidi Yekta contributed equally to this work. ✉email: gorjial@uni-muenster.de; Sahabnegahs@mums.ac.ir; sahabsajad@yahoo.com

resemble the ECM, researchers can promote the growth and differentiation of NSCs, as well as the development of new neural tissue¹⁷. Among the various hydrogels, self-assembling peptides (SAPs) like RADA16 have gained attention for their potential therapeutic applications in TBI¹⁸. These peptides form nanofiber scaffolds that mimic the ECM of brain, providing physical support for injured tissue and promoting cellular attachment, migration, and differentiation^{19,20}. Previous studies demonstrated that combining SAPs with functional motifs could enhance outcomes in animal models of TBI²¹. In our previous study, rats treated with RADA16-IKVAV showed increased neuron survival and decreased inflammation compared to untreated controls²². In another study, mice with TBI treated with a SAP functionalized with a nerve growth factor mimetic exhibited facilitated axonal growth and subsequent functional recovery²³. These findings suggest that using SAPs like RADA16 in combination with functional motifs represents a promising therapeutic strategy for TBI²².

Stromal cell-derived factor 1 (SDF-1) is a chemokine that plays a critical role in a variety of physiological and pathological processes, including immune cell migration, stem cell homing, and tissue repair²⁴. SDF-1 is known for its ability to enhance neural progenitor cells (NPCs) migration to injury sites, promote cell survival, and facilitate tissue repair^{25,26}. SDF-1 exerts these effects by binding to its receptor CXCR4, which is expressed on the surface of NPCs and promotes their migration to the site of injury^{27,28}. This chemotactic effect, coupled with ability of SDF-1 to promote neuroprotective effects such as neuronal survival, axonal growth, and synaptogenesis, makes it an ideal candidate for enhancing NSC behavior in neural tissue engineering^{26–31}. Based on our prior success in combining functional motifs of laminin (e.g., IKVAV) with RADA16²², we hypothesize that linking RADA16 to a functional motif of SDF-1 could enhance the beneficial effects of RADA16 on NSCs following TBI and may also facilitate the synaptogenesis of NSCs at the site of injury.

In this study, we introduce a novel approach by developing a nano-scaffold based on the self-assembling peptide RADA16 combined with a functional motif derived from SDF-1. This represents a significant advancement in the design of nano-scaffolds, as we have identified a functional motif capable of binding with the backbone scaffold, potentially enhancing stem cell integration and synaptogenesis at the injury site. Our results suggest that this nano-scaffold could significantly improve neural tissue repair following TBI, offering new perspectives on the design and application of nanomaterials for regenerative medicine and neuroscience.

Materials and methods

Study design

In this study, we designed a novel nano-scaffold based on the self-assembling peptide RADA16 and a functional motif of SDF-1 (RADA4-GG-KPVSLSYRCPCCRFFESHIARA; Nano-SDF). Then, we compared some biological properties of the Nano-SDF with our previous nano-scaffold (i.e., RADA4-GGS-IKVAV; R-GS1K) in *in vitro* conditions. To assay biological functions, we injected the Nano-SDF in a TBI model and evaluated behavioral, cellular, and molecular parameters regarding neuroinflammation and synaptogenesis.

Scaffold design and synthesis

The RADA16 was linked to the functional motif of SDF-1 (KPVSLSYRCPCCRFFESHIARA) using GG to increase the strength and stability of the scaffold. To identify the β sheet structure of Nano-SDF, the possible three-dimensional (3D) structure was assessed by an online system supported by Zhang lab (<https://zhanggroup.org/I-TASSER/>). Both scaffolds were synthesized by GL Biochem Ltd (Shanghai, China) with a purity of > 98%, which was measured via mass spectroscopy and high-performance liquid chromatography (HPLC).

Characterization of Nano-SDF

Hydrogel formation assay

To demonstrate hydrogel formation, the nano-peptide was subjected to two different conditions. In the first scenario, the Nano-SDF powder was mixed with deionized water in a microtube, while in the second, a 1% solution of the Nano-SDF was made in PBS. Hydrogel formation was compared between the two conditions.

Attenuated total reflectance Fourier transfer infrared spectroscopy (ATR-FTIR)

To investigate the chemical structure of the synthesized Nano-SDF, ATR-FTIR spectroscopy was used (Nicolet™ iS20 ATR-FTIR Spectrometer, Thermo Scientific, USA) over a range of 1200–2000 cm^{-1} . ATR-FTIR analysis of the Nano-SDF was performed on peptides dissolved at a concentration of 1% (w/v) in distilled water after 24 h incubation at 4 °C.

Gas chromatography-mass spectrometry (GC-Mass) and HPLC

The analysis of chemical compounds of nanofibers, such as molecular weight and polar materials, was assessed by gas chromatography coupled with mass spectrometry (Agilent 5975 C type, made in the USA). The current study established and validated a simple and sensitive HPLC method to determine Nano-SDF. The HPLC system consisted of an LC-10AD pump and an SPD10-Avp ultraviolet (UV) detector (Shimadzu, Japan). The UV absorbance of the sample (10 μL) was measured at the wavelength of 220 nm. Sample separation was performed on a Dikma Platsil C18-BIO column (250 mm × 4.6 mm) at 30 °C. The mobile phases for chromatographic separation included 0.1% Trifluoroacetic Acid in 100% Acetonitrile (Solvent A) and 0.1% Trifluoroacetic Acid in 100% Water (Solvent B) at a flow rate of 1.0 mL/min. Data acquisition and processing were performed using Shimadzu LC-Solution software.

Analysis of Nano-SDF by scanning electron microscope (SEM)

To investigate the surface morphology of the synthesized SDF-1 nanofibers, field emission SEM (FE-SEM) was performed. The Nano-SDF powder was dissolved in deionized water and prepared at a concentration of 1%. The homogenized solution contained 200 μl of PBS (pH=7.2), which was added for 1 h and then dried at

room temperature. After the gold-coating of the Nano-SDF, their microstructural was examined using energy dispersive spectroscopy (EDS) (Oxford Instrument, UK) for detecting carbon, oxygen, and nitrogen atoms related to the components of the nanofiber scaffold.

Nano-indentation

A nano-indentation experiment was carried out by an electromagnetic force application to a pendulum-based depth-sensing system called the AFM nano-indentation Test (Micro Materials, UK). A nano-indentation experiment was conducted to analyze the mechanical properties of the Nano-SDF. Initially, a gel sample was prepared by dissolving the Nano-SDF in water at a concentration of 1% w/v. The solution was then sonicated for at least 30 min and kept at room temperature until it became viscous. To initiate the gelation process and the formation of a network structure involving β -sheet aggregation, 0.5 mL of phosphate-buffered saline (PBS) with a pH of 7.4 was gently applied to the top of the peptide solution. After allowing the sample to stand for 1 h, the PBS was removed, and the resulting hydrogel was used in the nano-indentation experiment. The mechanical properties of the Nano-SDF were investigated and compared using a method adapted from Seyedkarimi and colleagues³². Specifically, different experimental designs were employed to analyze the mechanical properties of the two materials. The investigation revealed that the mechanical properties of the Nano-SDF were unaffected by the presence of ions from PBS. Moreover, adding ions led to new network structures with higher elastic modulus. It is important to note that changing the ionic strength and electrostatic interactions can significantly impact the properties of peptide hydrogels^{32,33}.

In vitro assay

Cell culture

Rat embryonic NSCs were isolated from ganglionic eminences on day 13 post-gestation and expanded using the neurosphere method^{34,35}. NSCs cultured in Dulbecco's Modified Eagle Medium/Nutrient Mixture F-12 (DMEM/F-12) (Gibco, Germany) containing 1.5% fetal bovine serum (FBS) (Gibco, Germany), 0.5% penicillin-streptomycin (Pen/Strep) (Gibco, Germany), 0.5% L-Glutamine (Gibco, Germany), 0.5% B27 (Gibco, Germany), 0.25% N2 (Gibco, Germany), 0.05% epidermal growth factor (EGF) (Sigma, Germany) to reach the 70% confluences. Neurospheres were formed in 5–7 days, and the cells were passaged. NSCs were obtained from the third to fifth passage and then transferred to 96-well and 6-well plates for further analysis.

Evaluation of proliferation and apoptosis of NSCs

In a 96-well plate, 2×10^4 NSCs/well were seeded and suspended in 100 μ L of the medium for the proliferation assay ($n=5$ for each group)^{20,36}. The R-GSIK and Nano-SDF scaffolds were applied in concentrations of 0.1% and 0.15% (w/v), respectively, to culture plates. After discarding the culture medium in each well, NSCs were treated with 20 μ L of MTS solution (5 mg/mL, Abcam; ab197010) that was pipetted into each well and incubated at 37 °C for 4 hours. Finally, a microplate reader set to 495 nm measured the optical density (OD) value³⁵.

Cell apoptosis was analyzed using the Caspase-Glo[®] 3/7 kit (Promega, USA). NSCs were seeded 2×10^4 NSCs/well of 96-well plates ($n=5$ for each group), and the R-GSIK and Nano-SDF scaffolds were applied to the culture plates at a concentration of 0.1% and 0.15% (w/v), respectively. Then, the culture medium (80 μ L) was discarded, and 100- μ L caspase solution was added at 37 °C for 3 h. The culture medium (80 μ L) was added to the plates^{35,37}. Finally, the OD value was measured. The MTS and caspase 3/7 assays were repeated on days 1, 5, and 10^{35,38}. The medium was changed every 2–3 days, and three parallel replicates were read for each sample.

Cell adhesion assay

For cell adhesion analysis, 2×10^4 NSCs were seeded in 6-well plates and allowed to adhere for 2 h³⁵. The R-GSIK and Nano-SDF scaffolds were applied to the 6-well plates at a concentration of 0.1% and 0.15%, respectively. Cells were then washed three times with PBS and fixed with 4% paraformaldehyde. The cell nuclei were stained with propidium iodide (PI). The attached cells were then observed with a fluorescent inverted phase contrast microscope.

Migration and neurite outgrowth assays

The R-GSIK and Nano-SDF scaffolds were injected on 6-well plates ($n=5$ for each group) at 0.1% and 0.15% (w/v) for the analysis of NSCs migration. The scaffolds had been coated in the center of each well, and a scaffold-free (Two-dimensional: 2D) environment had been created around the coated scaffolds. The coated portion of the well was then injected with 2×10^4 NSCs. On days 2 and 4, the migration of NSCs to the plate area without the scaffold was observed using a fluorescent inverted phase contrast microscope. Furthermore, 3 days following the implantation of NSCs onto the scaffolds, images were captured of the scaffold region. In each group, 10 cells were randomly selected, and the average value of cell axons was measured.

Immunocytochemistry

Immunocytochemistry was performed on day 7 of the study against SOX2 as a marker for NSCs (1:100, Sigma, Germany), nestin as a marker for neural stem/progenitor cells (1:150, Santa Cruz, Germany), Olig2 as a marker for oligodendrocytes (1:150; Millipore, Germany), and GFAP as a marker for astrocytes (1:150, Millipore, Germany) to compare the differentiation capacity of NSCs in normal culture (scaffold-free 2D environment) and culture with the R-GSIK and Nano-SDF scaffolds, respectively. The secondary antibody was fluorescein isothiocyanate (FITC) goat anti-rabbit (1:1000, Abcam, USA). Afterward, PI (1:1000, Sigma, Germany) was used to counterstain the nuclei.

In vivo assay

Animal care

A total of 60 adult male Wistar rats (220–250 g) at 8 weeks of age were purchased from the Animal Laboratory of Mashhad University of Medical Sciences. All animal experiments were approved by the Animal Ethics Committee of Mashhad Medical University, Iran, and were performed under the supervision of the National Institutes of Health Guide for the Care and Use of Laboratory Animals. The authors complied with the ARRIVE guidelines. Animals were kept under standard conditions (12 h light/dark cycle in a constant temperature environment of 22–24 °C) and had free access to water and food ad libitum. All methods were performed in accordance with the relevant guidelines and regulations.

TBI model and experimental groups

We have utilized a TBI model induction as previously described³⁹. After deep anesthesia by intraperitoneal (i.p.) administration of ketamine (80 mg/kg) and xylazine (10 mg/kg), rats were fixed in a stereotaxic frame (WPI, USA). A rectangular window was drilled into the skull bone above the M1/M2 cortex (A-P = from -1.5 mm to +1.5 mm; M-L = from -0.2 mm to -3 mm). The cavity was created by inserting a rotary biopsy punch (2 mm in diameter; Miltex, USA). All surgical procedures were performed under sterile conditions. Subsequently, the rats were randomly divided into six different groups, as described in Table 1.

Behavioral studies

Modified neurological severity scores (mNSS) assay The mNSS is a standard neurological scale used in animal studies and is determined through four tests: motor function, sensory function, balance, and reflexes. The mNSS score ranges from 0 to 18, and a higher score indicates a greater degree of neurological impairment⁴⁰. In our study, mNSS scoring was performed on day one before the TBI and on days 1, 8, 15, 22, and 29 after the TBI^{22,41}.

Open field assay The open field test is a well-established model to assess general motor function and anxiety levels. Before sacrificing the rats, we conducted an open field test on day 32 to analyze their general motor activity²². The device consists of a box (100 cm x 100 cm) with a camera placed above the center of the box. The total distance traveled can be recorded using a computer connected to the camera. The behavior of each animal was observed for 10 min after being placed in the center of the box. Before examining each rat, the field was thoroughly cleaned with water and a mild detergent to remove any lingering olfactory cues. In the examination room, the temperature, noise level, and lighting were all controlled⁴².

Elevated plus-maze (EPM) assay Anxiety-related behavior was assessed on days 16 and 32 following the injury⁴³. The EPM apparatus is an elevated 4-arm maze (50 cm, 50 cm, 5 cm) with two open arms (no walls) and two closed arms (20 cm dark, high walls), with a relative height of 60 cm from the ground. Each animal was placed in the maze's center, facing the close arm, and given five minutes to explore. A camera mounted above the maze kept track of each rat's time in open arms (OA) and the number of times they entered open arms (OAE). Two trials took place before the injury, and two more did so following it²².

Immunohistochemistry (IHC)

Following previously described procedures, immunohistochemistry was performed on paraffin-embedded coronal section⁴⁴. After deep anesthesia with ketamine and xylazine, perfusion was performed with 1 M phosphate-buffered saline. Brain tissue was transferred to 70%, 80%, 95% alcohol, 100% alcohol twice, xylene twice, and paraffin three times and then stored at 4 °C. After deparaffinization, the slices were incubated with 3% H2O2 for 30 min to inactivate endogenous peroxidases. The primary antibody against GAD65 (SC-377145, Santa Cruz; 1:10), PSD95 (ab18258, Abcam; 1:100), and synaptophysin (ab14692, Abcam, 1:20) was used overnight at 4 °C. The slices were washed three times in PBS, incubated for 1 h with goat anti-rabbit HRP (1:100, Abcam, USA) for 10 min, and counterstained with hematoxylin. To analyze the expression of each marker, we assessed four areas: the lesional area, the perilesional area, the extralesional area, and the contralateral area. The lesional area refers to the center of the injured site, while the perilesional area corresponds to the margin of the injured site. The extralesional area is approximately 100 micrometers away from the edge of the injury site. Lastly, the contralateral area refers to the opposite side of the injured cortex, specifically the intact cortex (Supplementary Figure A).

| Group and sample size | Intervention |
|------------------------------|---|
| Sham (N=10) | The rats underwent profound anesthesia, after which an incision was made on the skin covering their skull, and the incision was subsequently sutured. |
| TBI (N=10) | Induction of TBI |
| TBI + PBS (N=10) | Induction of TBI and injection of PBS as a vehicle for stem cells and scaffold |
| TBI + Nano-SDF (N=10) | Induction of TBI and injection of Nano-SDF |
| TBI + NSCs (N=10) | Induction of TBI and transplantation of 5×10^5 NSCs |
| TBI + Nano-SDF + NSCs (N=10) | Induction of TBI, Nano-SDF injection, and transplantation of 5×10^5 NSCs. |

Table 1. Summary of animal groups.

Quantitative RT-PCR

Total RNA was extracted with a total RNA extraction kit (Pars tous-151001). Quality control and quantification of total purified RNA were performed in triplicate by a NanoDrop2000 spectrophotometer (Thermo Fisher Scientific, MA). Synthesize cDNA using the Simple cDNA Reverse Transcription Kit (Pars tous-5301142). Primers were designed based on PubMed GenBank and were synthesized by Metabion International AG (Munich, Germany). Primer sequences are listed in Table 2. Quantitative RT-PCR was performed using qPCR SYBR Green master mix (Ampliqon-A323402-25), and real-time PCR was performed in a thermal cycler (Lightcycler System; Roche Diagnostics Corp., Indianapolis, IN, USA).

Data analysis

Data were analyzed with GraphPad Prism 8.0. Behavioral data were analyzed by repeated measures analysis of variance (ANOVA) to identify significant differences between different time points. However, we analyzed differences between groups by one-way ANOVA followed by Tukey's post hoc test for the other tests. All data are expressed as the mean \pm standard error of the mean (SEM). $P < 0.05$ was considered as a statistical significance.

Results

Characterization of Nano-SDF scaffold

Bioinformatics data

To design a nano-scaffold, we first analyzed computational methods to predict the secondary structure and solvent accessibility. Briefly, the prediction of the secondary structure was evaluated with an overall confidence value of about five and above in the attached motif, indicating a high degree of confidence in the accuracy of the predicted secondary structure. Analysis of predicted solvent accessibility revealed that about 40% of the polypeptide residues are exposed to the solvent, and the bioactive motif of the attached SDF-1 has an acceptable exposure to the solvent, indicating a high level of accessibility. These results provide important insights into the synthesized polypeptide's potential interactions and functional properties (Fig. 1A)⁴⁵. The structure predictions showed that the helix length and peptide folding properties of RADA16 were intact and consistent with the previously described structure of RADA16 (Fig. 1B)^{46,47}.

GC-mass and HPLC

The prepared SDF-1 nanofibers had two peaks with a base ion (mass/charge number of ions; m/z) at 1060.05 and 1413.10. The molecular weight of the SDF-1 nanofibers was \sim 4235.74 g/m, and the molecular weight of (RADA16) was \sim 1671.75 g/m. Based on these data, the identity of the SDF-1 nanofibers was confirmed by analysis in a mass spectrometer (Fig. 1C). Data from HPLC results demonstrated that the purity of the Nano-SDF was about $> 99\%$ for 25 min of assessment (Fig. 1D).

Hydrogel formation

A comparison of hydrogel formation under different conditions revealed that the Nano-SDF maintained its hydrogel form at the bottom of the inverted microtube when a 1% Nano-SDF solution was prepared in PBS. (Fig. 1E)

ATR-FTIR

When analyzing the amide I region ($1600\text{--}1700\text{ cm}^{-1}$), mainly associated with the C=O stretching vibration, the nanofibers showed β -sheet features characterized by the presence of the two components at 1630 and 1695 cm^{-1} , as expected. Moreover, the peaks in the region of the amide II ($1480\text{--}1575\text{ cm}^{-1}$) confirmed the β -sheet aggregation at 1530 cm^{-1} (directly related to CN stretching and NH bending). The typical peaks of RADA16 are visible in the spectrum of the Nano-SDF, indicating that the β -sheet structure of the backbone is essential for the self-assembly of Nano-SDF (Fig. 2A). The spectrum of the Nano-SDF is slightly sharper and broader compared to the spectrum of RADA16, and the β -sheet aggregation is also shifted somewhat, which

| Gene symbol | Forward primer 5' >> 3' Reveres primer 3' << 5' | T _A (°C) annealing temperature |
|-----------------------|--|--|
| Nestin | FCTCGGGAGTGTGCGCTTAGAG RATCTTGAGGTGTGCCAGTTG | 63 |
| SOX2 | FCCCCACCTACAGCATGTCCTA RTGGAGTGGGAGGAAGAGGTA | 55 |
| IFN- γ | FTGAGCATGCCAAGTTCGAG RTCTGGTGACAGCTGGTGAATC | 55 |
| TNF- α | FAGGCTGTCGCTACATCACTG RCTCTCAATGACCCGTAGGGC | 61 |
| IL-1 β | FGACTTCACCATGGAACCCGT RGGAGACTGCCATTCTCGAC | 60 |
| DCX | FGCTGACCTGACTCGATCCTT RCCGACCAGTTGGATTGACAT | 59 |
| Act β (Control) | FGCGCAAGTACTCTGTGTGG RCATCGTACTCTGCTTGTG | 60 |

Table 2. Primer sequences and annealing temperatures.

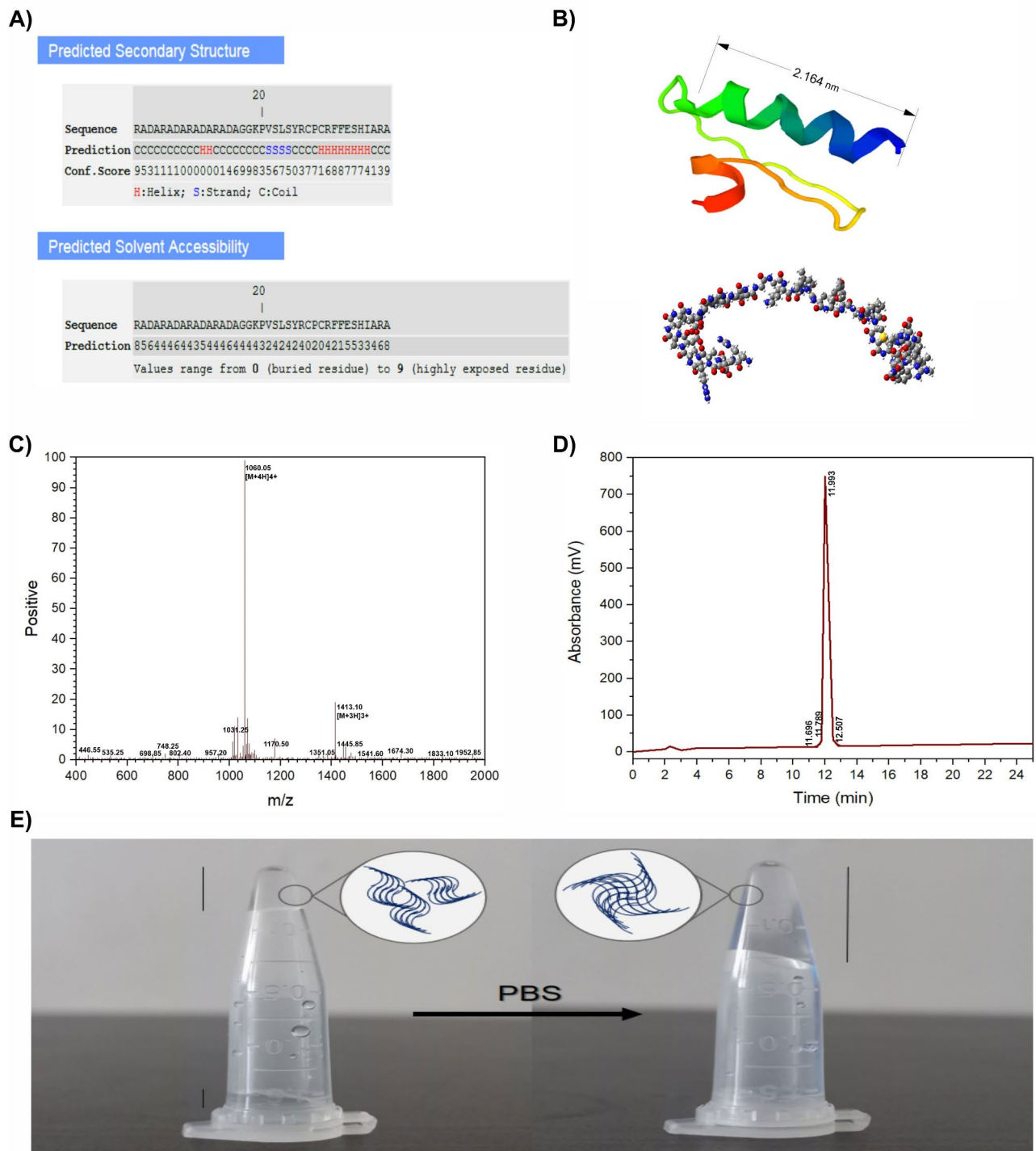


Fig. 1. (A) Prediction of β -sheet structure and solvent accessibility of Nano-SDF. (B) Visualization of the 3D β -sheet structure and solvent accessibility of Nano-SDF. (C) Representative GC-MS data for the nanofiber (Nano-SDF). Key mass/charge (m/z) peaks at 1060.05 $[M + 4 H] + 4$ and 1413.10 $[M + 3 H] + 3$, confirming the molecular identity of the nanofibers. Additional peaks correspond to various molecular fragments. The molecular weight of the nanofibers was estimated to be ~ 4235.74 g/mol, aligning with the expected molecular weight of the scaffold. (D) A representative HPLC chromatogram was obtained for the nanofiber (Nano-SDF). Two major peaks with retention times of 11.693 and 12.257 min, indicating a purity of over 99%. The analysis confirms the high purity and stability of the synthesized nanofibers within a 25-minute assessment window. (E) SDF-1 nanofibers formed a gelatinous material after the addition of an ion solution (PBS).

may be due to the molecular structure and integrity of the linkage sequence. The network structure of RADA16 is conserved in the Nano-SDF, showing the relationship between RADA16 and the linked sequence.

SEM

The nanostructures of the Nano-SDF fibers were first investigated using SEM. The Nano-SDF exhibited porous structures of about 200–400 nm, as revealed by FE-SEM (Fig. 2B). AFM confirmed that the Nano-SDF could self-assemble and create 3D microenvironments⁴⁸ at a physiological pH and osmolarity as previously described. AFM also picked up on the interconnected nanostructure network of the Nano-SDF. As expected, the diameter of the Nano-SDF fibers was about 30 nm, as observed by AFM²¹. By selecting random locations in the FE-SEM images of the Nano-SDF nanofibrous samples, the EDS spectra revealed multiple signals of carbon, oxygen, and nitrogen atoms associated with the components of the nanofibrous scaffolds. These results indicate that these components are uniformly distributed in the scaffolds' pore walls (Fig. 2C).

Nano-SDF indentation

The AFM nano-indentation technique investigated the synthesized Nano-SDF's mechanical properties, and the changes in force and displacement are shown in Fig. 2D, E. The displacement was consistently around ~ 250 nm during the initial application of force up to 60 μ N. Subsequently, as depicted in the diagram, the displacement decreased with increasing power from 60 μ N up to the maximum pressure of 145.97 μ N in the Nano-SDF configuration. The elastic modulus of the Nano-SDF synthesized scaffold was 3.21 KPa, calculated from the stress-strain curve in Fig. 2D, E using the Oliver-Pharr method⁴⁹. In addition, in supplementary Table A, a summary of studies comparing gray and white matter moduli in the central nervous system is reported for comparison with the synthesized Nano-SDF scaffold. Our findings demonstrated that the nanofiber structure exhibited greater porosity on the surface, while the internal structure was denser and more robust. The nanofiber scaffold's surface presented a network design and more cavities, which were more conducive to cell growth and penetration. In contrast, the dense and sturdy design of the nanofiber scaffold trunk could withstand more significant weight and flexibility against physical changes. These results also confirmed the β -sheet aggregation of the nanofiber scaffold, which was stacked like grids and thicker in the center for added strength and cohesion (Fig. 2D, E).

Biological activity of nano-SDF in vitro

In vitro biocompatibility assay

Our data indicated that Nano-SDF had no toxicity properties on cell viability detected by MTS assay compared to the control groups (Fig. 2F). We also observed that Nano-SDF did not induce any apoptotic responses in NSCs assessed by Caspase 3/7 compared to the 2D and R-GSIK groups (Fig. 2G). Our results proved that Nano-SDF was safe for stem cells and did not produce a toxic response upon prolonged exposure during in vitro expansion (i.e., ten-day assessments).

Initial cell attachment

The initial step in a cascade of cell-material interactions (e.g., cell guidance, migration, and differentiation) is cell attachment. To this point, we first compared the initial cell adhesion capacity between the Nano-SDF and our previous nano-scaffold (the R-GSIK). We demonstrated that the initial number of cells was significantly attached to the Nano-SDF compared to the R-GSIK (Fig. 3A; $P < 0.01$).

Neurite outgrowth and migration

Since SDF-1 is involved in neuronal migration and neurite outgrowth, we next determined whether a bioactive of SDF-1 conjugated with RADA16 (the Nano-SDF) contributes to NSCs-mediated migration and neurite length. Our results demonstrated that the neurite length of NSCs was significantly increased when encapsulated in the Nano-SDF scaffold compared to the R-GSIK scaffold (Fig. 3B; $P < 0.05$).

Another promising finding, as shown in Fig. 3C, was that the migration of NSCs was significantly enhanced in the Nano-SDF scaffold compared to the R-GSIK scaffold at 2 and 4 days of cultivation ($P < 0.05$).

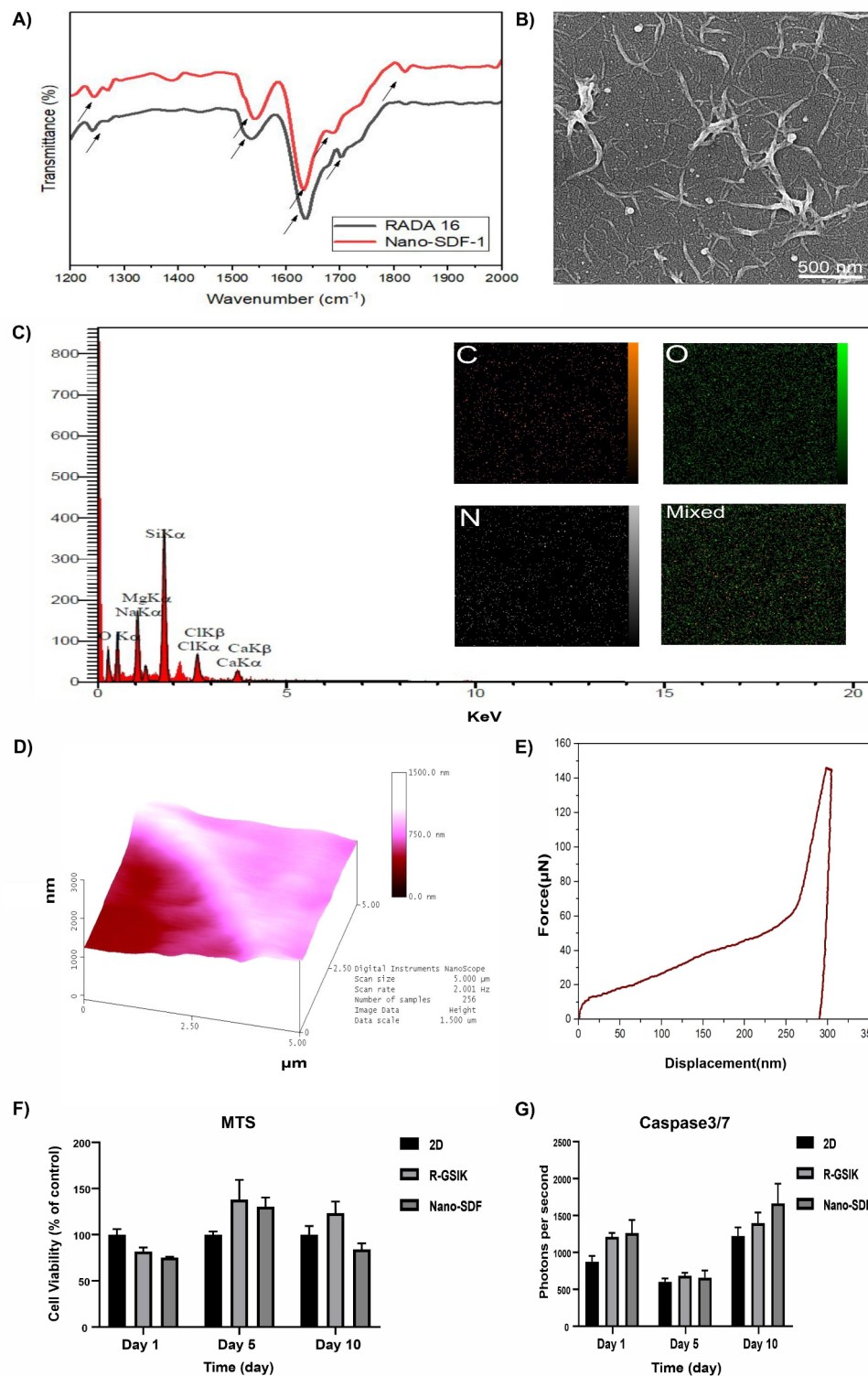
Cellular differentiation

We found that nestin, a neural progenitor marker, was significantly increased in the Nano-SDF group compared to the 2D and R-GSIK groups (Fig. 4; $P < 0.01$). There were no significant differences in the expression of SOX2 between the groups. Further analysis showed that the expression of Olig2 was significantly decreased in the Nano-SDF group compared to the R-GSIK group (Fig. 4; $P < 0.05$). However, our results indicated that the expression of GFAP, an astrocyte marker, was significantly decreased in the R-GSIK group compared to the 2D culture (Fig. 4; $P < 0.01$).

Outcomes of nano-SDF application in vivo

Sensorimotor improvement

The sensorimotor assessment was evaluated by mNSS test 1, 8, 15, 22, and 29 days after the injury. Our results showed that the mNSS score was significantly improved in the NSCs group compared to the TBI group on 1, 15, 22, and 29 days after injury (Fig. 5, panel 1 A; $P < 0.01$). Furthermore, the mNSS score decreased considerably at 8 and 15 days after TBI in the NSCs group compared to the TBI + PBS as a vehicle group (Fig. 5, panel 1 A; $P < 0.05$). Interestingly, mNSS as a functional recovery parameter was significantly improved in the Nano-SDF group compared to the control groups (i.e., TBI and TBI + PBS groups) on 15 and 29 (Fig. 5, panel 1 A; $P < 0.05$). Our results indicated that the combination group (Nano-SDF plus NSCs) improved the mNSS score compared to the TBI group on days 1, 8, 15, and 29 after injury (Fig. 5, panel 1 A; $P < 0.01$). Moreover, the Nano-



SDF + NSCs-treated group had better functional recovery than the TBI + PBS group on days 8, 15, and 22 after injury. No significant difference was observed in the total distance traveled between the groups as an indicator of gross locomotor activity (Fig. 5, panel 1B).

Anxiety-like behavior

Our results demonstrated that the number of open arm entries was significantly increased in the TBI-NSCs group compared to the TBI and TBI-Nano-SDF groups on day 32 after injury ($P < 0.05$; Fig. 5, panel 1C). On day 16 after TBI, the time spent in the open arm was significantly higher in the TBI-Nano-SDF group compared to the TBI group ($P < 0.05$; Fig. 5, panel 1C).

Fig. 2. (A) ATR-FTIR spectra of RADA16 and Nano-SDF. The arrows in the figure indicate key wavenumber regions corresponding to the characteristic peaks of β -sheet structures, including amide I (1630 and 1695 cm^{-1}) and amide II (1530 cm^{-1}), which are essential for confirming the β -sheet aggregation in the Nano-SDF and RADA16. (B) FE-SEM image of the prepared nanofiber scaffold (Nano-SDF) in the horizontal direction. (C) EDS point analysis for the elemental composition of the nanofiber scaffold (Nano-SDF). The mapping images on the right display the spatial distribution of key elements, including carbon (C), oxygen (O), and nitrogen (N). The Mixed map highlights the overall elemental composition. These results confirm the presence of elements essential for the nanofiber scaffold structure. (D) Representative 3D AFM images of the nanofiber (Nano-SDF). AFM nano-indentation topography of Nano-SDF hydrogel, showing the 3D surface morphology. The scan size is $5\text{ }\mu\text{m} \times 5\text{ }\mu\text{m}$, with a height scale up to 1500 nm , revealing the nanoscale topography and structural integrity of the hydrogel. The color gradient from dark red to light pink represents surface height variations, with darker regions corresponding to lower surface heights and lighter regions to higher surface heights. (E) The load-displacement response obtained from indenting nanofiber (Nano-SDF) splats deposited onto the substrate at $25\text{ }^{\circ}\text{C}$ using a Berkovich indenter, showing the indentation depth and final displacement of 298.08 nm . The curve demonstrates the relationship between the applied force and the resulting displacement in the material, with a maximum force of $\sim 145.97\text{ }\mu\text{N}$ and displacement reaching approximately 300 nm . The elastic modulus of the Nano-SDF was calculated to be 3.21 KPa , confirming the scaffold's mechanical properties and its suitability for mimicking the stiffness of neural tissue. (F, G) A comparison of the biocompatibility properties of Nano-SDF using MTS (F) and Caspase 3/7 (G) assays shows that the Nano-SDF did not exhibit any toxicity toward the NSCs. Furthermore, the data indicate that the Nano-SDF did not induce an apoptotic response in the NSCs. The results are presented as the mean \pm SEM.

Neurogenesis markers at the mRNA level

We evaluated the expression levels of SOX2, nestin, and doublecortin (DCX) at the injury site to assess neurogenesis markers. Our results showed that the expression of nestin and DCX (a marker of immature neuronal cells) was significantly higher in the combination group (TBI-Nano-SDF with NSCs) compared to the TBI-NSCs group (Fig. 5, panel 2B and 2 C; $P < 0.05$). We also observed an increase in the level of nestin in the combination group compared to the TBI-Nano-SDF and TBI-NSCs groups (Fig. 5, panel 2B; $P < 0.05$). Furthermore, nestin expression was significantly higher in the sham and TBI groups compared to the TBI-Nano-SDF and TB-NSCs (Fig. 5, panel 2B; $P < 0.01$).

Neuroinflammatory markers at the mRNA level

To identify the anti-inflammatory effects of the Nano-SDF in combination with NSCs following TBI, several proinflammatory cytokines (i.e., IL-1 β , IFN- γ , and TNF- α) were assessed at the mRNA level. Our findings revealed that there were significantly lower IFN- γ levels in the combination group (TBI-Nano-SDF with NSCs) in comparison to the sham group (Fig. 5, panel 2E; $P < 0.05$). However, there was no significant difference between groups on the mRNA expression levels of IL-1 β and TNF- α .

The effects of Nano-SDF on synaptogenesis at injury site

Our data showed that the expression of PSD-95 in the TBI groups (i.e., TBI, TBI + PBS, TBI + Nano-SDF, and TBI + NSCs) was significantly increased in comparison to the sham group in lesional and perilesional areas (Fig. 6; $P < 0.001$). Surprisingly, the expression of PSD-95 was significantly decreased in lesional and perilesional areas when rats were treated with the Nano-SDF plus NSCs compared to TBI groups (i.e., TBI, TBI + PBS, TBI + Nano-SDF, and TBI + NSCs) (Fig. 6; $P < 0.01$), indicating a normalization of excitatory synaptic activity. There was no significant difference between the sham and the combination group (Nano-SDF + NSCs) in lesional and perilesional areas, indicating that levels of PSD-95 returned to normal levels. In the extralesional area, PSD-95 was significantly higher in the TBI + Nano-SDF and TBI + NSCs compared to the TBI + PBS (Fig. 6; $P < 0.01$). We also did not observe any significant changes between groups in the expression of PSD-95 in contralateral areas (Fig. 6).

Our results also showed that the expression of GAD-65 was considerably increased in the TBI and TBI + PBS groups in lesional areas compared to the sham group (Fig. 7; $P < 0.05$). Furthermore, a high level of GAD-65 was observed in the TBI + NSCs group compared to the sham group (Fig. 7; $P < 0.05$). On the other hand, we found that the TBI + Nano-SDF and the TBI + Nano-SDF + NSCs significantly decreased the protein expression of GAD-65 in lesional areas compared to the TBI group (Fig. 7; $P < 0.05$), indicating a potential restoration of the excitatory-inhibitory balance. In contrast, the level of GAD-65 was dramatically increased in the TBI + Nano-SDF group compared to the TBI + NSCs, TBI + Nano-SDF + NSCs, and sham groups in the perilesional area (Fig. 7; $P < 0.01$). There was no significant difference between the groups in the expression of GAD-65 in extralesional and contralateral areas.

Our data indicated that synaptophysin expression was significantly increased in all TBI groups compared to the sham group in the lesional area (Fig. 8; $P < 0.001$). Notably, the Nano-SDF treatment significantly decreased synaptophysin expression in the lesional regions compared to the TBI group (Fig. 8; $P < 0.05$), suggesting improved synaptic function. However, there was no significant difference between the groups in synaptophysin expression in the perilesional, extralesional, and contralateral areas.

Discussion

This study found that the synthesized nano-scaffold containing SDF-1 enhances NSC behavior in a TBI model.

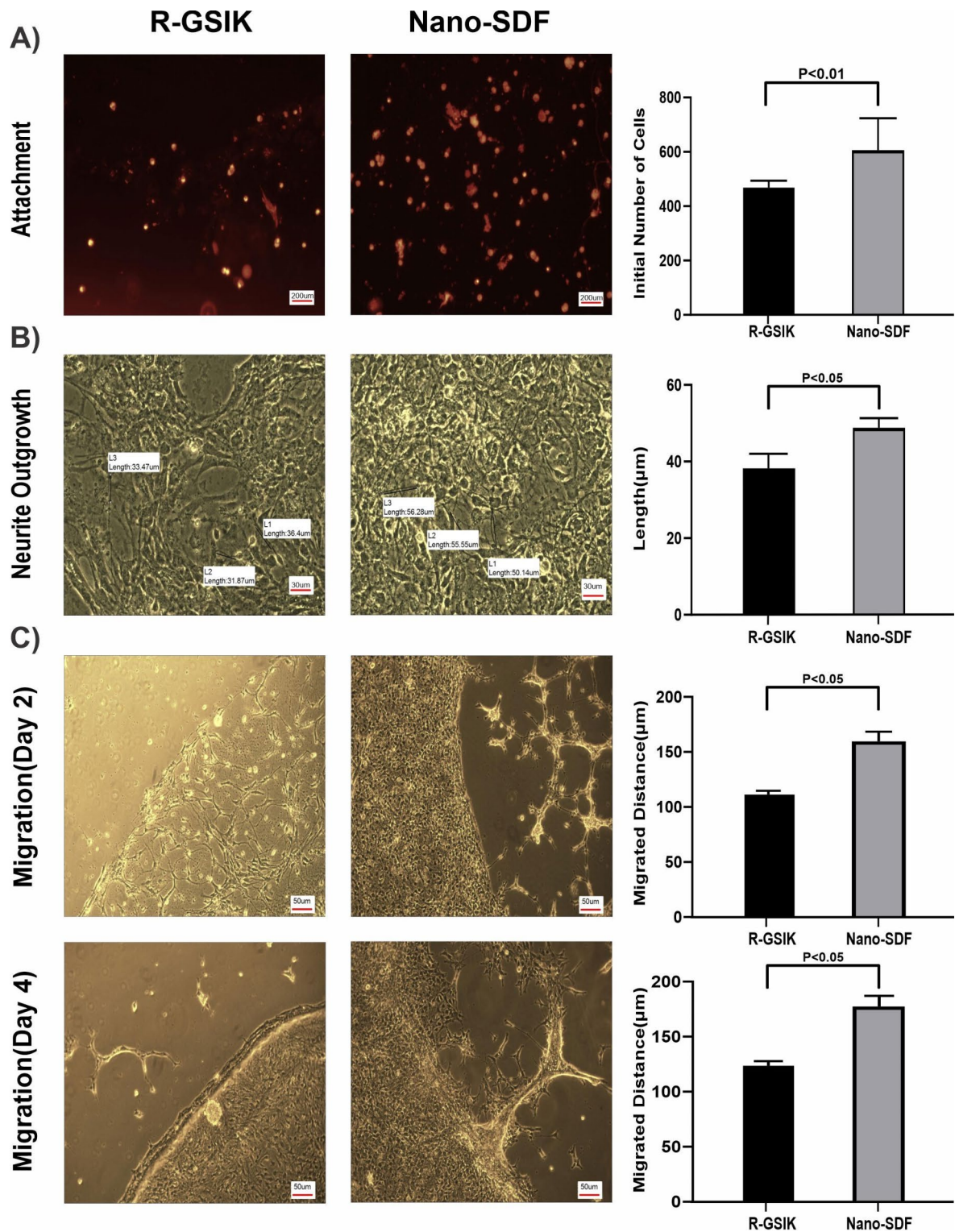


Fig. 3. (A, B) Assessment of initial cell attachment and neurite outgrowth of NSCs on culture medium containing Nano-SDF and R-GSIK showed that the Nano-SDF significantly improved cell attachment and neurite outgrowth of NSCs compared to R-GSIK. (C) Assessment of NSC migration on culture medium containing Nano-SDF and R-GSIK on days 2 and 4 showed that the Nano-SDF significantly improved cell migration compared to R-GSIK. The results are presented as the mean \pm SEM.

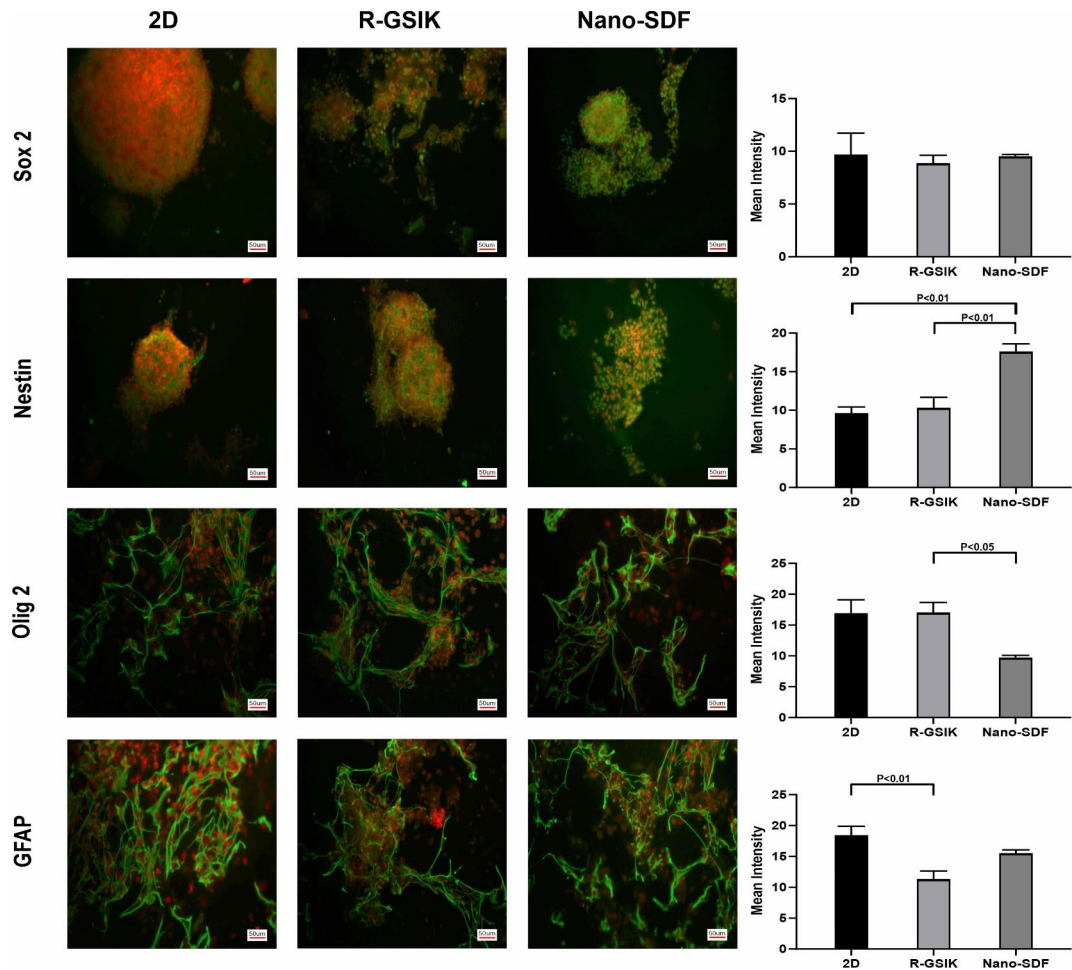


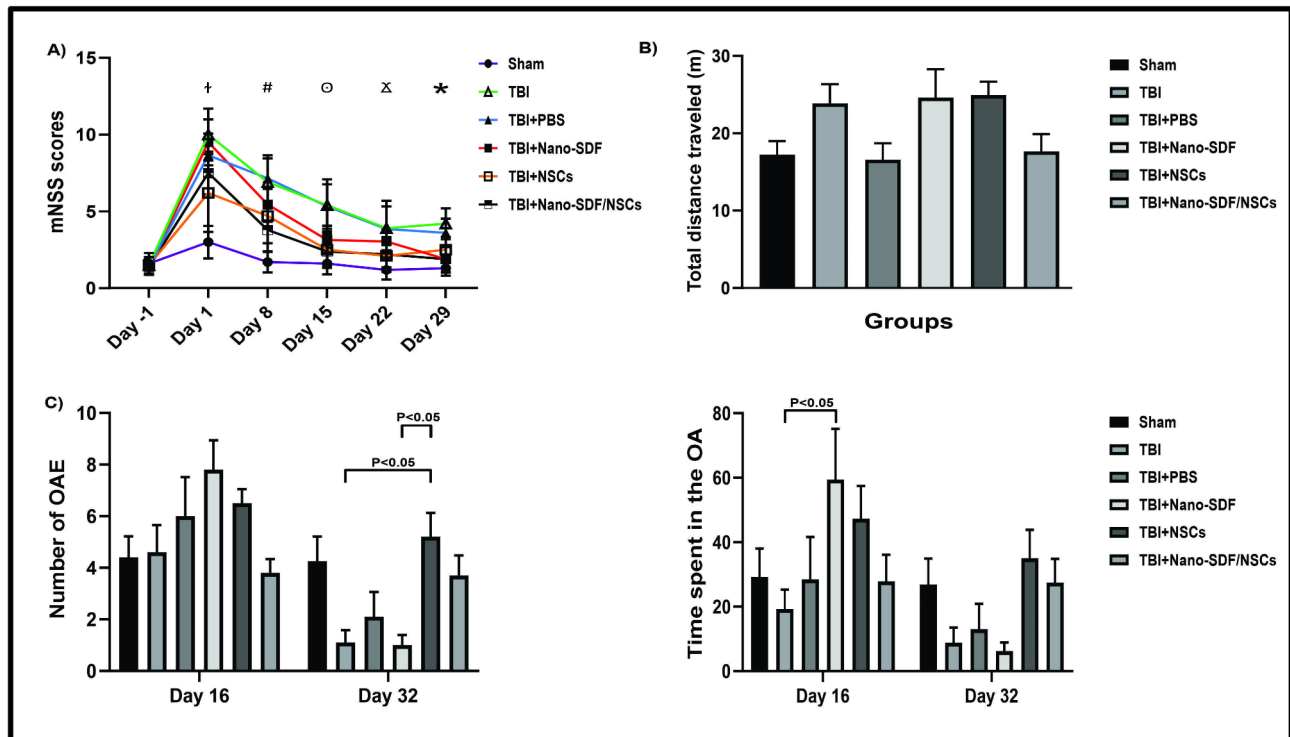
Fig. 4. NSC differentiation was assessed by immunostaining nestin, SOX-2, Olig2, and GFAP (green) after seeding on Nano-SDF and R-GSIK and in a 2D environment. Immunofluorescent staining was conducted on the NSCs after 7 days of differentiation, with cell nuclei stained using Propidium iodide (PI; red). The results are presented as the mean \pm SEM.

Our analysis confirms that the β -sheet aggregation of the Nano-SDF contributes to the scaffold's structural integrity, ensuring adequate support for NSCs⁵⁰. SEM revealed the interconnected nanostructure network of the Nano-SDF, with a fiber diameter of approximately 30 nm. This nanostructure mimics the ECM of neural tissue and could potentially provide a conducive environment for NSC adhesion, proliferation, and differentiation. The high surface area-to-volume ratio of the nano-scaffold allows extensive cell-scaffold interaction, which is essential for effective tissue regeneration^{35,44,51,52}.

The mechanical properties of the scaffold could greatly influence cellular behavior and tissue regeneration. Young's elastic modulus of SAP hydrogels used in neural tissue engineering is an important parameter that can affect cell behavior and tissue regeneration⁵³. To better contextualize the nano-indentation results, the findings of previous studies characterizing the mechanical properties of gray and white matter in the central CNS were summarized (Supplementary Table A). The Young's elastic modulus of SAPs can vary depending on the specific type of SAP and its concentration^{53,54}. Recently, to improve the mechanical stability of the RADA16 peptide hydrogel, two different forms of RADA16 were conjugated with an Arg-Gly-Asp sequence and a photocrosslinkable diacrylated poly(-caprolactone)-b-poly(ethylene glycol)-b-poly(-caprolactone) triblock copolymer⁵⁵. Notably, it is well-established that cells are sensitive to the mechanical cues provided by their microenvironment and that scaffolds with a stiffness similar to the target tissue could promote desirable cellular responses, such as improved attachment, migration, and differentiation^{56,57}. The synthesized nano-scaffold exhibited an elastic modulus of 3.21 KPa, which closely aligns with the mechanical properties of intact neural tissue (Supplementary Table A). This is a critical parameter, as the stiffness and elasticity of the scaffold must match the target tissue to provide optimal support for cell growth and function^{58–62}.

In the context of neural tissue engineering, scaffolds with appropriate mechanical properties could provide a supportive and biomimetic environment for NSCs and other neural cells, thereby enhancing their survival, proliferation, and integration within the injured tissue. This was particularly relevant for treating TBI, where restoring functional neural connections posed a critical challenge. By designing the Nano-SDF scaffold with an elastic modulus that closely matched the stiffness of native neural tissue, we aimed to create a biomimetic

Panel 1: Behavioral Assessments



Panel 2: Molecular Assessments

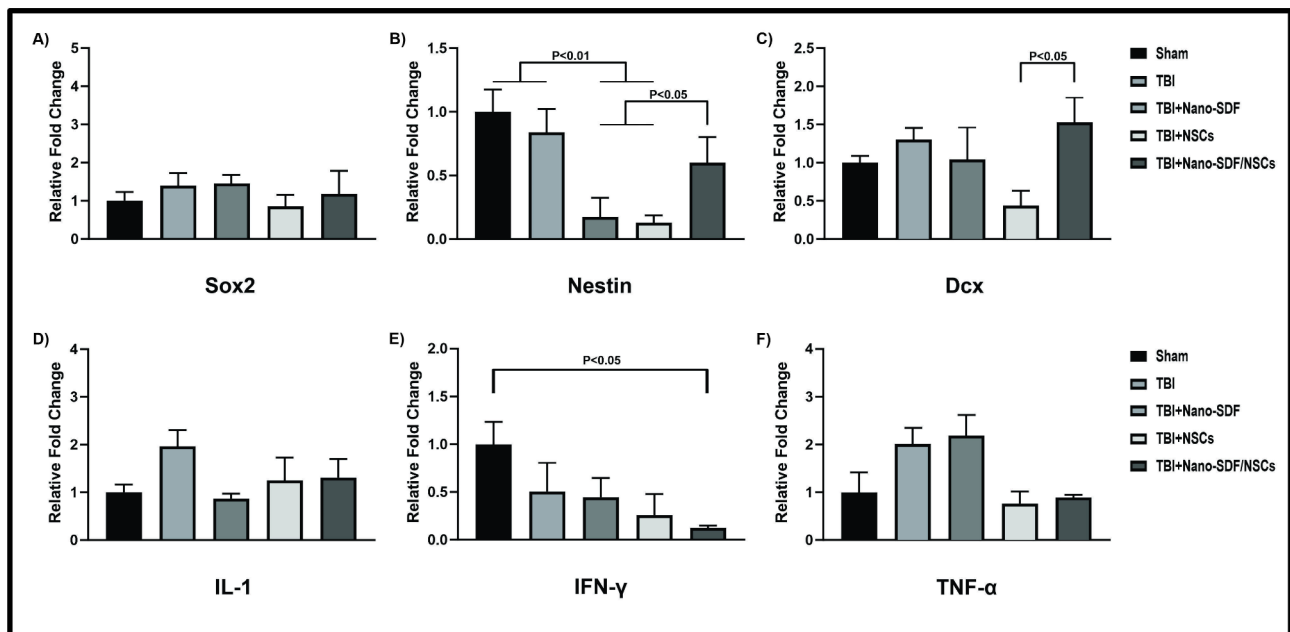


Fig. 5. Panel 1: Behavioral evaluations were conducted to assess motor function and anxiety-like behavior in animals. Motor function was assessed using the modified Neurological Severity Score (mNSS) and Open Field tests (A, B), while anxiety-like behavior was measured by analyzing the time spent by animals on the open and closed arms of the Elevated Plus Maze (EPM) (C). The results are presented as the mean \pm SEM. The following symbols indicate statistical significance: $P < 0.05$ between NSCs vs. TBI and Nano-SDF + NSCs vs. TBI groups on day 1 (#). $P < 0.05$ between Nano-SDF + NSCs vs. TBI, NSCs vs. TBI+PBS, and NSCs vs. TBI+PBS on day 8 (#). $P < 0.05$ between NSCs vs. TBI, NSCs vs. TBI+PBS, Nano-SDF vs. TBI, Nano-SDF vs. TBI+PBS, and Nano-SDF + NSCs vs. TBI on day 15 (○). $P < 0.05$ between NSCs vs. TBI, Nano-SDF vs. TBI, and Nano-SDF vs. TBI+PBS on day 22 (Δ). $P < 0.05$ between NSCs vs. TBI, Nano-SDF vs. TBI, Nano-SDF vs. TBI+PBS, and Nano-SDF + NSCs vs. TBI on day 29 (*). Panel 2: Quantitative RT-PCR analysis was conducted to assess the mRNA expression levels of SOX2, nestin, and DCX as markers of neurogenesis (A, B, C), and IL-1 β , IFN- γ , and TNF-alpha as markers of neuroinflammation (D, E, F). The results are presented as the mean \pm SEM.

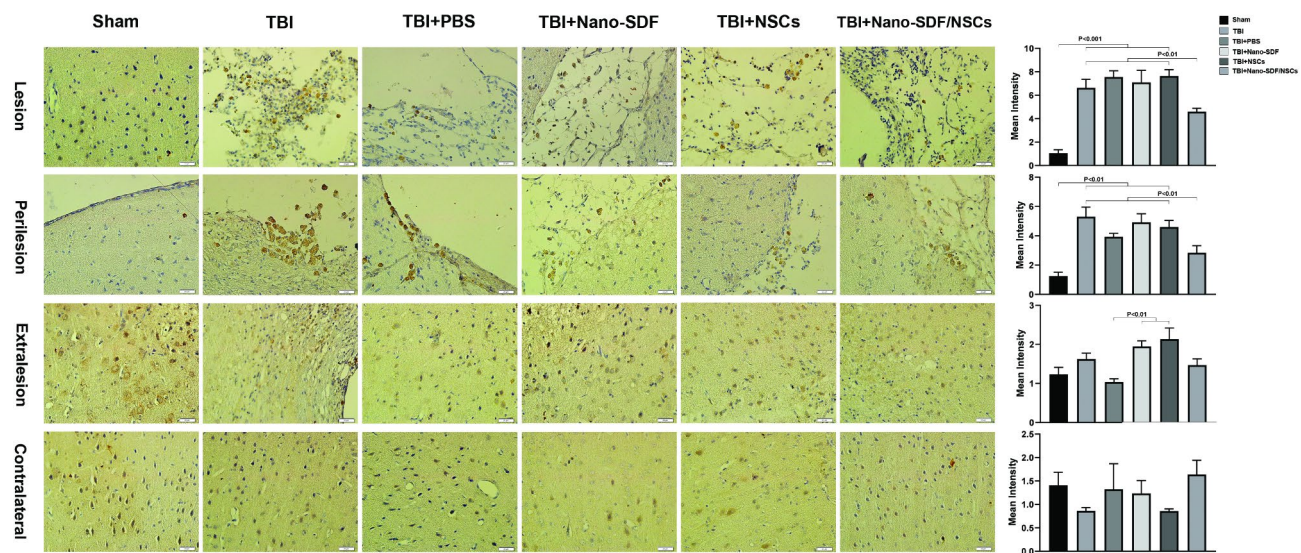
PSD 95

Fig. 6. The expression of postsynaptic density 95 (PSD95) was evaluated by immunohistochemistry (IHC) at four areas of each slide, namely lesional, perilesional, extralesional, and contralateral, in different experimental groups. In the combination group (Nano-SDF + NSCs), the expression of PSD95 was similar to the sham group in the lesional and perilesional areas. The results are presented as the mean \pm SEM.

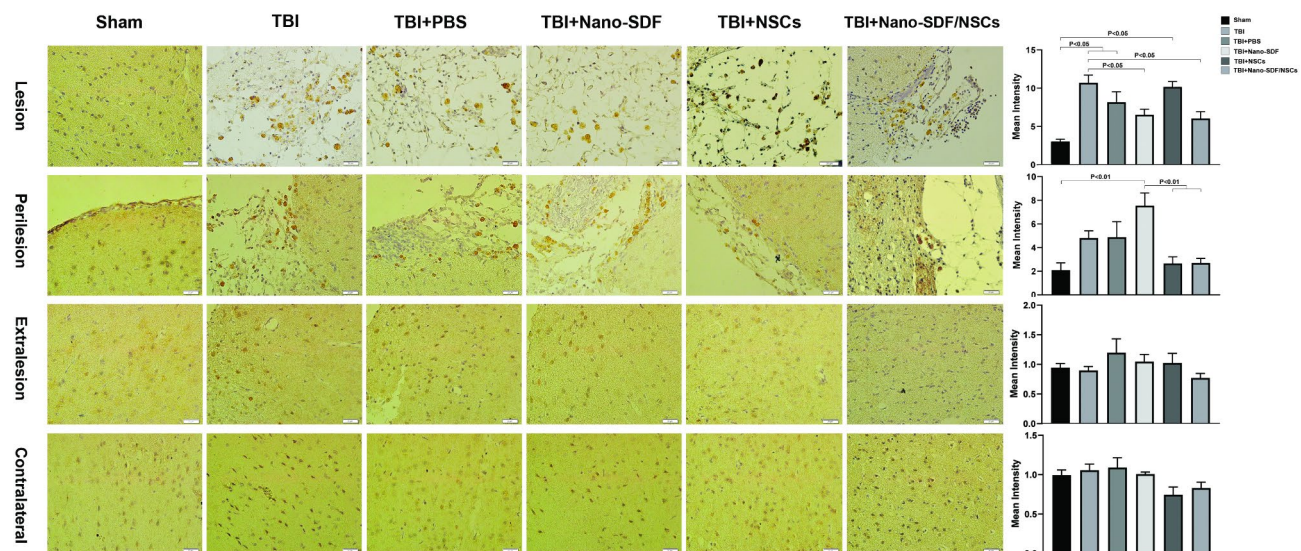
GAD65

Fig. 7. The expression of a 65-kilodalton isoform of glutamic acid decarboxylase (GAD65) was evaluated using immunohistochemistry (IHC) at four different regions on each slide, which included the lesional, perilesional, extralesional, and contralateral areas, in various experimental groups. The results are presented as the mean \pm SEM.

microenvironment that could better support the growth and maturation of NSCs and the formation of functional synaptic connections. Our findings demonstrate that this design approach significantly enhanced the overall effectiveness of the Nano-SDF scaffold in promoting neural tissue regeneration and functional recovery following TBI.

Nano-scaffolds used in neural tissue engineering possess several essential characteristics. Firstly, they should be biocompatible and biodegradable, meaning they do not cause adverse reactions and can be safely absorbed by the body over time^{63,64}. To ensure the novel Nano-SDF was safe for NSCs, we evaluated its cytotoxicity,

Synaptophysin

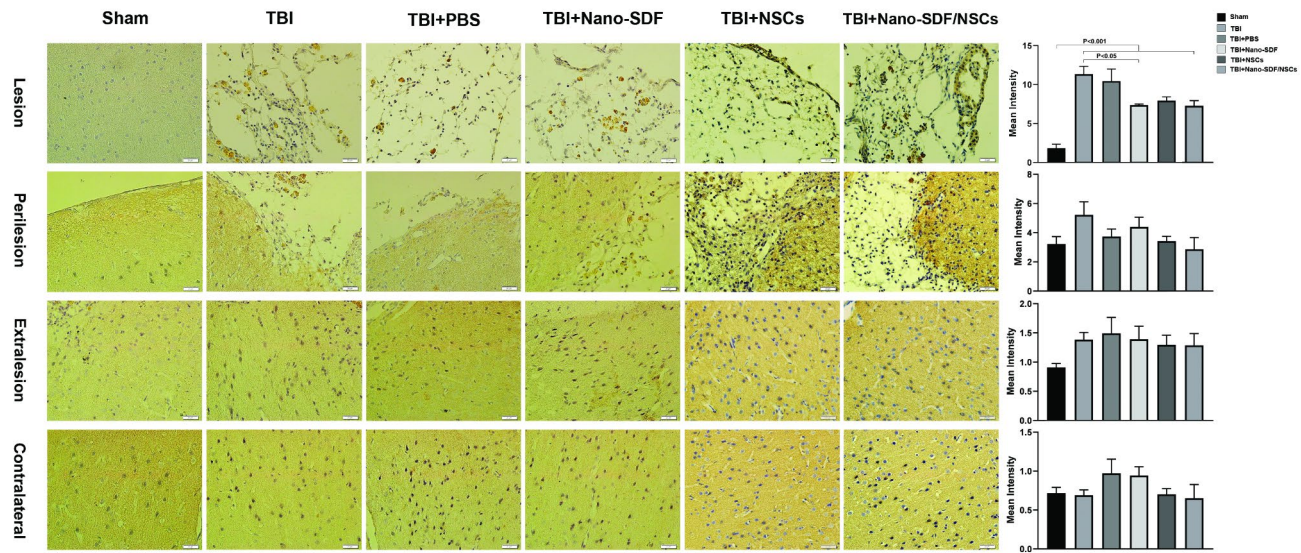


Fig. 8. The expression of synaptophysin was evaluated using immunohistochemistry (IHC) at four different regions on each slide, which included the lesional, perilesional, extralesional, and contralateral areas in different experimental groups. The results are presented as the mean \pm SEM.

comparing survival rates and apoptosis with those induced by the R-GSIK. Our study demonstrated the safety of Nano-SDF for stem cells, revealing no induction of a toxic response during prolonged *in vitro* expansion. This result is consistent with several studies showing that nano-scaffold biomaterials, inspired by SAPs, possess outstanding biocompatibility, biodegradability, and a microenvironment that mimics the ECM^{51,65–68}.

Inducing synaptogenesis by SAPs holds excellent potential for improving outcomes for patients with TBI^{69,70}. For instance, a recent study found that a new type of SAP scaffold could be a substrate for neurite outgrowth and synapse formation⁷¹. Our analysis also demonstrated that the Nano-SDF could support neurite outgrowth *in vitro* and the formation of functional synapses *in vivo*. Furthermore, Nano-scaffolds should promote cell adhesion, proliferation, and differentiation, facilitate controlled release of bioactive molecules for enhanced cell behavior and tissue regeneration, and have a high surface area-to-volume ratio, allowing extensive cell-scaffold interaction^{62,72–76}. Our data shows that Nano-SDF significantly enhances the initial cell adhesion, migration, and differentiation of NSCs, which are crucial processes in neural regeneration, compared to the R-GSIK. This aligns with earlier observations, which showed that SAPs could mimic the natural ECM, enhancing various cells' attachments, growth, and differentiation^{71,77,78}. This improvement can be attributed to the scaffold's ability to provide a supportive biomechanical environment that promotes synaptogenesis and functional recovery. This study supports earlier evidence that SDF-1 enhances the survival, migration, and differentiation of NSCs, which are essential for brain development and repair^{79–81}. In sum, our novel nano-scaffold incorporated a functional motif of SDF-1 in an innovative three-dimensional milieu, providing a supportive environment for cell growth and function.

As previously demonstrated in a TBI model, the Nano-SDF modulates neuroinflammatory pathways and apoptosis. The findings suggest that the Nano-SDF has the potential as a tool for promoting synaptogenesis and neuronal regeneration through mitigating neuroinflammation and apoptosis^{21,48}. Our findings also revealed a significant difference in IFN- γ between the combination group (Nano-SDF with NSCs) and the sham group. Our study showed no significant differences in IL-1 β and TNF- α mRNA levels between groups. This suggests that the anti-inflammatory effects of the Nano-SDF and NSCs combination may specifically target specific cytokines, like IFN- γ . The significant reduction in IFN- γ , a key mediator of neuroinflammation and a contributor to TBI pathology, indicates a potential therapeutic benefit of this combination in reducing neuroinflammatory responses^{82,83}. While IL-1 β and TNF- α levels remained unchanged, the decrease in IFN- γ potentially highlights the selective modulation of inflammatory pathways and supports further exploration of this treatment for TBI⁸⁴. Furthermore, the behavioral parameters significantly improved in groups treated with NSCs and the Nano-SDF compared to the control groups.

Accumulating evidence has highlighted the strong association of TBI with an imbalance of excitation and inhibition tone in the injured brain, like GAD-65^{85,86}. For example, the total levels of PSD-95, the primary scaffold protein at excitatory synapses, increased after a controlled cortical impact. PSD-95 plays a significant role in mediating intracellular signaling by synaptic N-methyl-D-aspartate (NMDA) subtype glutamate receptors. It has conclusively been shown that TBI accumulates synaptophysin at injured sites, a marker of synaptic vesicle transportation and synaptic function⁸⁷. To get a comprehensive view of synaptic connections after intervening in TBI, we assessed GAD-65, PSD-95, and synaptophysin in different areas of the experimental groups. The most remarkable result from our data was that synaptogenesis markers were improved considerably when rats

were treated with stem cells and the Nano-SDF. These findings collectively suggest that the novel nano-scaffold containing SDF-1 enhances NSC behavior and synaptogenesis and restores the excitatory-inhibitory balance in the injured brain. This balance is crucial for maintaining proper neural network function post-injury and may underlie the observed functional recovery⁸⁸. Future studies should further explore the long-term effects of this treatment on excitatory-inhibitory balance and neural network function. Using Nano-SDF in neural tissue engineering could promote regeneration after TBI and provide a supportive environment for cell growth and function.

While our study highlights the potential of a novel nano-scaffold containing SDF-1 to enhance NSC behavior and promote synaptogenesis after TBI, several limitations must be acknowledged. The study focuses on short-term effects, with long-term impacts and recovery's durability requiring further investigation. Potential side effects, such as immune responses, were not comprehensively evaluated, highlighting the need for additional safety studies. The small sample size may limit the generalizability of the findings, and the rodent model may not fully replicate human TBI, emphasizing the need for larger animal models and clinical trials. Further studies should include additional control groups, such as different concentrations of SDF-1, and explore the specific contributions of SDF-1 and its molecular mechanisms to understand better the pathways involved.

In summary, the Nano-SDF, with optimal mechanical stability, cytocompatibility, and no toxic agents for NSCs, exhibited superior effects on cell behavior—enhancing attachment, neurite outgrowth, and differentiation. Furthermore, it significantly improved synaptogenesis, signifying functional improvements in a TBI model. Further studies are needed to assess the potential application of this innovative nano-scaffold in enhancing cell regeneration and facilitating brain repair following TBI.

Data availability

The data that support the findings of this study are available on request from the corresponding authors.

Received: 23 April 2024; Accepted: 6 January 2025

Published online: 17 February 2025

References

1. Capizzi, A., Woo, J. & Verduzco-Gutierrez, M. Traumatic brain injury: An overview of epidemiology, pathophysiology, and medical management. *Med. Clin.* **104** (2), 213–238 (2020).
2. Thapa, K. et al. Traumatic brain injury: Mechanistic insight on pathophysiology and potential therapeutic targets. *J. Mol. Neurosci.* **71** (9), 1725–1742 (2021).
3. Ng, S. Y. & Lee, A. Y. W. Traumatic brain injuries: Pathophysiology and potential therapeutic targets. *Front. Cell. Neurosci.* **13**, 528 (2019).
4. Weston, N. M. & Sun, D. The potential of stem cells in treatment of traumatic brain injury. *Curr. Neurol. Neurosci. Rep.* **18**, 1–10 (2018).
5. Cao, H., Liu, T. & Chew, S. Y. The application of nanofibrous scaffolds in neural tissue engineering. *Adv. Drug Deliv. Rev.* **61** (12), 1055–1064 (2009).
6. Gu, X. Progress and perspectives of neural tissue engineering. *Front. Med.* **9**, 401–411 (2015).
7. Gu, X., Ding, F. & Williams, D. F. Neural tissue engineering options for peripheral nerve regeneration. *Biomaterials* **35** (24), 6143–6156 (2014).
8. Shajkumar, A. *Future of Nanotechnology in Tissue Engineering, in Nanotechnology Applications for Tissue Engineering* 289–306 (Elsevier, 2015).
9. Yang, L. et al. A biodegradable hybrid inorganic nanoscaffold for advanced stem cell therapy. *Nat. Commun.* **9** (1), 3147 (2018).
10. Cheng, T. Y. et al. Neural stem cells encapsulated in a functionalized self-assembling peptide hydrogel for brain tissue engineering. *Biomaterials* **34** (8), 2005–2016 (2013).
11. Bakhtiyari, N. et al. Advances in peptide-based hydrogel for tissue engineering. *Polymers* **15** (5), 1068 (2023).
12. Binaymotagh, R. et al. Peptide-based hydrogels: New materials for biosensing and biomedical applications. *Materials* **15** (17), 5871 (2022).
13. Li, Q. et al. Recent trends in the development of hydrogel therapeutics for the treatment of central nervous system disorders. *NPG Asia Mater.* **14** (1), 14 (2022).
14. Sankar, S. et al. Clinical use of the self-assembling peptide RADA16: A review of current and future trends in biomedicine. *Front. Bioeng. Biotechnol.* **9**, 679525 (2021).
15. Hlavac, N., Kasper, M. & Schmidt, C. Progress toward finding the perfect match: Hydrogels for treatment of central nervous system injury. *Mater. Today Adv.* **6**, 100039 (2020).
16. Madhusudanan, P., Raju, G. & Shankarappa, S. Hydrogel systems and their role in neural tissue engineering. *J. R. Soc. Interface.* **17** (162), 20190505 (2020).
17. Li, J. et al. Dual-enzymatically cross-linked gelatin hydrogel promotes neural differentiation and neurotrophin secretion of bone marrow-derived mesenchymal stem cells for treatment of moderate traumatic brain injury. *Int. J. Biol. Macromol.* **187**, 200–213 (2021).
18. Koss, K. & Unsworth, L. Neural tissue engineering: Bioreponsive nanoscaffolds using engineered self-assembling peptides. *Acta Biomater.* **44**, 2–15 (2016).
19. Shi, W. et al. Transplantation of RADA16-BDNF peptide scaffold with human umbilical cord mesenchymal stem cells forced with CXCR4 and activated astrocytes for repair of traumatic brain injury. *Acta Biomater.* **45**, 247–261 (2016).
20. Sahab Negah, S. et al. Laminin-derived ile-lys-val-ala-Val: A promising bioactive peptide in neural tissue engineering in traumatic brain injury. *Cell Tissue Res.* **371**, 223–236 (2018).
21. Hajinejad, M. et al. Exosomes and nano-SDF scaffold as a cell-free-based treatment strategy improve traumatic brain injury mechanisms by decreasing oxidative stress, neuroinflammation, and increasing neurogenesis. *Stem Cell. Reviews Rep.* **19** (4), 1001–1018 (2023).
22. Negah, S. S. et al. Transplantation of human meningioma stem cells loaded on a self-assembling peptide nanoscaffold containing IKVAV improves traumatic brain injury in rats. *Acta Biomater.* **92**, 132–144 (2019).
23. Lu, C. et al. Bioactive self-assembling peptide hydrogels functionalized with brain-derived neurotrophic factor and nerve growth factor mimicking peptides synergistically promote peripheral nerve regeneration. *ACS Biomaterials Sci. Eng.* **4** (8), 2994–3005 (2018).
24. Hajinejad, M. et al. Resveratrol pretreatment enhanced homing of SDF-1 α -preconditioned bone marrow-derived mesenchymal stem cells in a rat model of liver cirrhosis. *J. Cell. Biochem.* **119** (3), 2939–2950 (2018).

25. Zampronni, L. N. et al. Injection of SDF-1 loaded nanoparticles following traumatic brain injury stimulates neural stem cell recruitment. *Int. J. Pharm.* **519** (1–2), 323–331 (2017).
26. Ho, S. Y. et al. SDF-1/CXCR4 signaling maintains stemness signature in mouse neural stem/progenitor cells. *Stem Cells Int.* **2017** (1), 2493752 (2017).
27. Zhu, C. et al. SDF-1 and CXCR4 play an important role in adult SVZ lineage cell proliferation and differentiation. *Brain Res.* **1657**, 223–231 (2017).
28. Cheng, X. et al. The role of SDF-1/CXCR4/CXCR7 in neuronal regeneration after cerebral ischemia. *Front. NeuroSci.* **11**, 590 (2017).
29. Tran, P. B. & Miller, R. J. Chemokine receptors in the brain: A developing story. *J. Comp. Neurol.* **457** (1), 1–6 (2003).
30. Liu, H. et al. Hypoxic preconditioning advances CXCR4 and CXCR7 expression by activating HIF-1 α in MSCs. *Biochem. Biophys. Res. Commun.* **401** (4), 509–515 (2010).
31. Honczarenko, M. et al. Human bone marrow stromal cells express a distinct set of biologically functional chemokine receptors. *Stem Cells.* **24** (4), 1030–1041 (2006).
32. Seyedkarimi, M. S., Mirzadeh, H. & Bagheri-Khoulenjani, S. On the analysis of microrheological responses of self-assembling RADA16-I peptide hydrogel. *J. Biomed. Mater. Res. Part. A.* **107** (2), 330–338 (2019).
33. Chau, Y. et al. Incorporation of a matrix metalloproteinase-sensitive substrate into self-assembling peptides—a model for biofunctional scaffolds. *Biomaterials* **29** (11), 1713–1719 (2008).
34. Azari, H. et al. Establishing embryonic mouse neural stem cell culture using the neurosphere assay. *J. Vis. Exp.* **47**, 2457. <https://doi.org/10.3791/2457> (2011).
35. Sahab Negah, S. et al. Enhancement of neural stem cell survival, proliferation, migration, and differentiation in a novel self-assembly peptide nanofibrous scaffold. *Mol. Neurobiol.* **54**, 8050–8062 (2017).
36. Akiyama, Y. et al. Transplantation of clonal neural precursor cells derived from adult human brain establishes functional peripheral myelin in the rat spinal cord. *Exp. Neurol.* **167** (1), 27–39 (2001).
37. Adelita, T. et al. Proteolytic processed form of CXCL12 abolishes migration and induces apoptosis in neural stem cells in vitro. *Stem Cell. Res.* **22**, 61–69 (2017).
38. Huat, T. J. et al. IGF-1 enhances cell proliferation and survival during early differentiation of mesenchymal stem cells to neural progenitor-like cells. *BMC Neurosci.* **15** (1), 91 (2014).
39. Aligholi, H. et al. Preparing neural stem/progenitor cells in PuraMatrix hydrogel for transplantation after brain injury in rats: A comparative methodological study. *Brain Res.* **1642**, 197–208 (2016).
40. Song, Y. M. et al. Differences in pathological changes between two rat models of severe traumatic brain injury. *Neural Regener. Res.* **14** (10), 1796–1804 (2019).
41. Chen, J. et al. Therapeutic benefit of intravenous administration of bone marrow stromal cells after cerebral ischemia in rats. *Stroke* **32** (4), 1005–1011 (2001).
42. Gould, T. D., Dao, D. T. & Kovacsics, C. E. The Open Field Test, in *Mood and Anxiety Related Phenotypes in Mice: Characterization Using Behavioral Tests*, T.D. Gould, Editor. 1–20 (Humana: Totowa, NJ, 2009).
43. Popovitz, J., Mysore, S. P. & Adwanikar, H. Long-term effects of Traumatic Brain Injury on anxiety-like behaviors in mice: behavioral and neural correlates. *Front. Behav. Neurosci.* **13**, 6. <https://doi.org/10.3389/fnbeh.2019.00006> (2019).
44. Jahanbazi Jahan-Abad, A. et al. Human neural Stem/Progenitor cells derived from epileptic human brain in a self-assembling peptide nanoscaffold improve traumatic brain injury in rats. *Mol. Neurobiol.* **55** (12), 9122–9138 (2018).
45. Zhao, X. & Zhang, S. Designer self-assembling peptide materials. *Macromol. Biosci.* **7** (1), 13–22 (2007).
46. Cormier, A. R. et al. Molecular structure of RADA16-I designer self-assembling peptide nanofibers. *Acs Nano.* **7** (9), 7562–7572 (2013).
47. Zhang, S. Discovery and design of self-assembling peptides. *Interface Focus.* **7** (6), 20170028 (2017).
48. Ghandy, N. et al. Co-transplantation of novel Nano-SDF scaffold with human neural stem cells attenuates inflammatory responses and apoptosis in traumatic brain injury. *Int. Immunopharmacol.* **115**, 109709 (2023).
49. Yan, W., Pun, C. L. & Simon, G. P. Conditions of applying Oliver–Pharr method to the nanoindentation of particles in composites. *Compos. Sci. Technol.* **72** (10), 1147–1152 (2012).
50. Novasodova, E. V. et al. Composite Coatings based on recombinant spidroins and peptides with motifs of the Extracellular Matrix proteins enhance neuronal differentiation of neural precursor cells derived from Human Induced Pluripotent Stem cells. *Int. J. Mol. Sci.* **24** (5), 4871 (2023).
51. Peressotti, S. et al. Self-assembling hydrogel structures for neural tissue repair. *ACS Biomaterials Sci. Eng.* **7** (9), 4136–4163 (2021).
52. Hasan, M. M. & Shahid, M. A. PVA, licorice, and collagen (PLC) based hybrid bio-nano scaffold for wound healing application. *J. Biomater. Sci. Polym. Ed.* **34** (9), 1217–1236 (2023).
53. Koch, F. et al. Mechanical characteristics of beta sheet-forming peptide hydrogels are dependent on peptide sequence, concentration and buffer composition. *Royal Soc. Open. Sci.* **5** (3), 171562 (2018).
54. Leon, E. J. et al. Mechanical properties of a self-assembling oligopeptide matrix. *J. Biomater. Sci. Polym. Ed.* **9** (3), 297–312 (1998).
55. Zhai, H. et al. Mechanically strengthened hybrid peptide-polyester hydrogel and potential applications in spinal cord injury repair. *Biomed. Mater.* **15** (5), 055031 (2020).
56. Koser, D. E. et al. CNS cell distribution and axon orientation determine local spinal cord mechanical properties. *Biophys. J.* **108** (9), 2137–2147 (2015).
57. Budday, S. et al. Mechanical properties of gray and white matter brain tissue by indentation. *J. Mech. Behav. Biomed. Mater.* **46**, 318–330 (2015).
58. Asghar, M. S. et al. Antioxidant, and enhanced flexible nano porous scaffolds for bone tissue engineering applications. *Nano Select.* **2** (7), 1356–1367 (2021).
59. Rojas-Murillo, J. A. et al. Physical, mechanical, and biological properties of fibrin scaffolds for cartilage repair. *Int. J. Mol. Sci.* **23** (17), 9879 (2022).
60. Wang, L. et al. Smart, elastic, and nanofiber-based 3D scaffolds with self-deploying capability for osteoporotic bone regeneration. *Nano Lett.* **19** (12), 9112–9120 (2019).
61. Sharma, P., Pal, V. K. & Roy, S. An overview of latest advances in exploring bioactive peptide hydrogels for neural tissue engineering. *Biomater. Sci.* **9** (11), 3911–3938 (2021).
62. Del Rahmani, A. et al. Recent advances in nano-scaffolds for tissue engineering applications: Toward natural therapeutics. *Wiley Interdiscip. Rev. Nanomed. Nanobiotechnol.* **15** (6), e1882 (2023).
63. Ma, Y. et al. The dual effect of 3D-printed biological scaffolds composed of diverse biomaterials in the treatment of bone tumors. *Int. J. Nanomed.* **18**, 293–305. <https://doi.org/10.2147/IJN.S390500> (2023).
64. Shahriar, S. S. et al. Next-generation 3D scaffolds for nano-based chemotherapeutics delivery and cancer treatment. *Pharmaceutics* **14** (12), 2712 (2022).
65. Faroni, A. et al. Self-assembling peptide hydrogel matrices improve the neurotrophic potential of human adipose-derived stem cells. *Adv. Healthc. Mater.* **8** (17), 1900410 (2019).
66. Li, J. et al. Recent advances of self-assembling peptide-based hydrogels for biomedical applications. *Soft Matter.* **15** (8), 1704–1715 (2019).
67. Chen, J. & Zou, X. Self-assemble peptide biomaterials and their biomedical applications. *Bioactive Mater.* **4**, 120–131 (2019).
68. Acar, H. et al. Self-assembling peptide-based building blocks in medical applications. *Adv. Drug Deliv. Rev.* **110**, 65–79 (2017).

69. Yaguchi, A. et al. Efficient protein incorporation and release by a jigsaw-shaped self-assembling peptide hydrogel for injured brain regeneration. *Nat. Commun.* **12** (1), 6623 (2021).
70. Zweckberger, K. et al. Self-assembling peptides optimize the post-traumatic milieu and synergistically enhance the effects of neural stem cell therapy after cervical spinal cord injury. *Acta Biomater.* **42**, 77–89 (2016).
71. Holmes, T. C. et al. Extensive neurite outgrowth and active synapse formation on self-assembling peptide scaffolds. *Proc. Natl. Acad. Sci.* **97**(12), 6728–6733 (2000).
72. Zhen Xu, H. & Su, J. Restoration of critical defects in the rabbit mandible using osteoblasts and vascular endothelial cells co-cultured with vascular stent-loaded nano-composite scaffolds. *J. Mech. Behav. Biomed. Mater.* **124**, 104831 (2021).
73. Piluso, S., Leonidakis, A. K. & Patterson, J. Novel polyethylene glycol hydrogels incorporating RADA16 peptides as in vitro tissue mimetics. In *Frontiers in Bioengineering and Biotechnology Conference Abstract: 10th World Biomaterials Congress*. (2016).
74. Rao, S. H. et al. Natural and synthetic polymers/bioceramics/bioactive compounds-mediated cell signalling in bone tissue engineering. *Int. J. Biol. Macromol.* **110**, 88–96 (2018).
75. Balakrishnan, B. Role of nanoscale delivery systems in tissue engineering. *Curr. Pathobiol. Rep.* **9** (4), 119–132 (2021).
76. Wang, R. et al. Design of a RADA16-based self-assembling peptide nanofiber scaffold for biomedical applications. *J. Biomater. Sci. Polym. Ed.* **30** (9), 713–736 (2019).
77. Ando, K. et al. Effects of a self-assembling peptide as a scaffold on bone formation in a defect. *PLoS ONE* **13** (1), e0190833 (2018).
78. Lee, S. et al. Self-assembling peptides and their application in the treatment of diseases. *Int. J. Mol. Sci.* **20** (23), 5850 (2019).
79. Chen, Y. et al. Curcumin promotes the proliferation, invasion of neural stem cells and formation of neurospheres via activating SDF-1/CXCR4 axis. *Folia Neuropathol.* **59** (2), 152–160 (2021).
80. Ma, S. et al. Sodium alginate/collagen/stromal cell-derived factor-1 neural scaffold loaded with BMSCs promotes neurological function recovery after traumatic brain injury. *Acta Biomater.* **131**, 185–197 (2021).
81. Zhu, Y., Wang, Y. & Lu, Z. Injection of stromal cell-derived factor-1 (SDF-1) nanoparticles after traumatic brain injury stimulates recruitment of neural stem cells. *J. Biomed. Nanotechnol.* **18** (2), 498–503 (2022).
82. Abd-El-Basset, E. M., Rao, M. S. & Alsaqqobi, A. Interferon-Gamma and Interleukin-1Beta enhance the secretion of brain-derived neurotrophic factor and promotes the survival of cortical neurons in brain injury. *Neurosci. Insights.* **15**, 2633105520947081 (2020).
83. Freire, M. A. M. et al. Cellular and molecular pathophysiology of traumatic brain injury: What have we learned so far? *Biology* **12** (8), 1139 (2023).
84. Galindo, A. N., Rubio, D. A. F. & Hettiaratchi, M. H. Biomaterial strategies for regulating the neuroinflammatory response. *Mater. Adv.* **5**(10), 4025–4054. <https://doi.org/10.1039/d3ma00736g> (2024).
85. Witkowski, E. D. et al. Rapid changes in synaptic strength after mild traumatic brain injury. *Front. Cell. Neurosci.* **13**, 166 (2019).
86. Witkin, J. M. et al. Mechanistic and therapeutic relationships of traumatic brain injury and γ -amino-butyric acid (GABA). *Pharmacol. Therapeut.* **256**, 108609 (2024).
87. Shoji, H. & Kibayashi, K. Changes in localization of synaptophysin following fluid percussion injury in the rat brain. *Brain Res.* **1078** (1), 198–211 (2006).
88. Ghatak, S. et al. Novel Therapeutic approach for excitatory/Inhibitory imbalance in Neurodevelopmental and neurodegenerative diseases. *Annu. Rev. Pharmacol. Toxicol.* **61** (61, 2021), 701–721 (2021).

Author contributions

S.S-N., M-A.B-T. , and M.S conceived of the presented original idea. M-A.B-T. and M.S developed the theory and performed the computations. S.S-N verified the analytical methods and performed analysis and interpretation of results. H.J-Y, M-A.B-T, and M.S performed Characterization and Nano-indentation of scaffold. M-A.B-T and M.S. carried out the in-vitro experiments. M.H (behavioural tests) and H.H-R (IHC tests) carried out the in-vivo experiments. M-A.B-T, H.J-Y, and H.H-R. designed the figures. All authors discussed the results and contributed to the final manuscript. All authors reviewed the results and approved the final version of the manuscript. A.G and S.S-N supervised the findings of this work. S.S-N and A.G Agreed to be accountable for all aspects of the work in ensuring that questions related to the accuracy or integrity of any part of the work are appropriately investigated and resolved.

Funding

This research did not receive any specific grant from funding agencies in the public, commercial, or not-for-profit sectors.

Declarations

Competing interests

The authors declare no competing interests.

Ethics approval and consent to participate

All animal experiments were approved by the Animal Ethics Committee of Mashhad Medical University, Iran, and were performed under the supervision of the National Institutes of Health Guide for the Care and Use of Laboratory Animals. The authors complied with the ARRIVE guidelines. All methods were performed in accordance with the relevant guidelines and regulations.

Consent for publication

Not applicable.

Additional information

Supplementary Information The online version contains supplementary material available at <https://doi.org/10.1038/s41598-025-85698-5>.

Correspondence and requests for materials should be addressed to A.G. or S.S.N.

Reprints and permissions information is available at www.nature.com/reprints.

Publisher's note Springer Nature remains neutral with regard to jurisdictional claims in published maps and institutional affiliations.

Open Access This article is licensed under a Creative Commons Attribution-NonCommercial-NoDerivatives 4.0 International License, which permits any non-commercial use, sharing, distribution and reproduction in any medium or format, as long as you give appropriate credit to the original author(s) and the source, provide a link to the Creative Commons licence, and indicate if you modified the licensed material. You do not have permission under this licence to share adapted material derived from this article or parts of it. The images or other third party material in this article are included in the article's Creative Commons licence, unless indicated otherwise in a credit line to the material. If material is not included in the article's Creative Commons licence and your intended use is not permitted by statutory regulation or exceeds the permitted use, you will need to obtain permission directly from the copyright holder. To view a copy of this licence, visit <http://creativecommons.org/licenses/by-nc-nd/4.0/>.

© The Author(s) 2025